OPEN ACCESS

Intermetallic charge transfer between A-site Cu and B-site Fe in A-site-ordered double perovskites

New Journal of Physics
The open-access journal for physics

Intermetallic charge transfer between A-site Cu and B-site Fe in A-site-ordered double perovskites

Youwen Long[1,2] **and Yuichi Shimakawa**[2]
Institute for Chemical Research, Kyoto University, Uji, Kyoto 611-0011, Japan
E-mail: ywlong@riken.jp and shimak@scl.kyoto-u.ac.jp

New Journal of Physics **12** (2010) 063029 (17pp)
Received 2 February 2010
Published 16 June 2010
Online at http://www.njp.org/
doi:10.1088/1367-2630/12/6/063029

Abstract. In this review article, we describe in detail the temperature-induced intermetallic charge transfer between A-site Cu and B-site Fe ions in the A-site-ordered double perovskites $R\mathrm{Cu_3Fe_4O_{12}}$ ($R = \mathrm{La}$, Bi). In these compounds, a very rare $\mathrm{Cu^{3+}}$ valence state at the square-planar-coordinated A sites was stabilized by high-pressure synthesis. By increasing the temperature, a Cu–Fe intermetallic charge transfer producing a high $\mathrm{Fe^{3.75+}}$ valence state occurred. This charge transfer gave rise to a first-order isostructural phase transition with unusual volume contraction, as well as to antiferromagnetism-to-paramagnetism and insulator-to-metal transitions. The substitution of Bi for La stabilized the low-temperature phase containing $\mathrm{Cu^{3+}}$ and increased the charge transfer transition temperature from 393 K for $\mathrm{LaCu_3Fe_4O_{12}}$ to 428 K for $\mathrm{BiCu_3Fe_4O_{12}}$.

[1] Present address: Multiferroics Project, ERATO, JST, c/o Cross-Correlation Materials Research Group (CMRG), ASI, RIKEN, Wako, Saitama 351-0198, Japan.
[2] Authors to whom any correspondence should be addressed.

Contents

1. Introduction

Transition metal (TM) oxides with perovskite and perovskite-like structures have attracted much attention owing to their wide varieties of physical properties, some of which are useful for technological applications. The octahedrally coordinated B sites in a simple ABO_3 perovskite are usually occupied by TM ions, and the physical properties of the perovskite are determined in large part by strong interactions between the TM ions as well as by the hybridization of TM 3d and oxygen 2p orbitals. The 12-fold-coordinated A sites, on the other hand, often accommodate relatively large ions, such as alkaline metal, alkaline-earth metal and rare earth ions. When three-quarters of the A-site cations are replaced by another element, an A-site-ordered double perovskite with a general chemical formula $A'A_3B_4O_{12}$ can be obtained. The crystal structure of such a double perovskite with cubic *Im*-3 symmetry is shown in figure 1. Because the BO_6 octahedra in this structure are significantly tilted (a typical B–O–B bond angle is about 140°), the A-site-ordered double perovskite has square-planar-coordinated AO_4 units rather than 12-fold-coordinated A sites like those in the simple ABO_3 perovskites.

Another interesting feature of oxides with this structure is that the square-coordinated A sites can accommodate TM ions like Jahn–Teller active Cu^{2+} and Mn^{3+}. Because there are TM ions at both the A and B sites in the structure, A–A and A–B interactions in addition to the B–B interaction seen in many simple perovskite oxides give the A-site-ordered double perovskites interesting physical properties [1, 2]. For example, giant dielectric constants ($\approx 10^5$) in a broad temperature region were found in $CaCu_3Ti_4O_{12}$ [3]–[5]. Large magnetoresistance under low applied fields was observed in a $CaCu_3Mn_4O_{12}$ ferrimagnetic semiconductor and $ACu_3Mn_4O_{12}$ (A = La, Bi) half metals, where A-site Cu and B-site Mn spins couple antiferromagnetically [6]–[8]. Either ferromagnetism or antiferromagnetism appears from the A–A magnetic interaction in $CaCu_3B_4O_{12}$ (B = Ge, Ti, Sn) [9, 10]. Progressive transitions due to charge, orbital and spin orderings occurred in $NaMn_3Mn_4O_{12}$ [11]. Also reported in the literature are antiferromagnetic interactions between Mn^{3+} ($S = 2$) spins at the A site in $YMn_3Al_4O_{12}$ [12] and magnetic-dielectric coupling in $BiMn_3Mn_4O_{12}$ [13, 14]. A recent experiment on $LaMn_3Ti_4O_{12}$ revealed that the A site can also be occupied by Mn with an unusually low valence state rather than by Jahn–Teller Mn^{3+} [15].

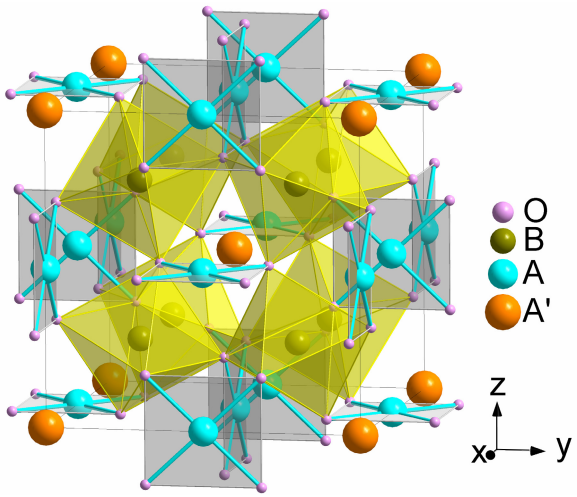

Figure 1. Crystal structure of A-site-ordered double perovskite $A'A_3B_4O_{12}$ with an *Im*-3 space group. Atomic sites: A′ 2*a* (0, 0, 0); A 6*b* (0, 0.5, 0.5); B 8*c* (0.25, 0.25, 0.25); O 24*g* (*x*, *y*, 0).

Very recently, a new phenomenon concerning the A–B intersite interaction was discovered in an A-site-ordered $LaCu_3Fe_4O_{12}$ double perovskite: Cu–Fe intermetallic charge transfer [16]. Different from chemical doping, which is a conventional way of modulating the valence states in TM oxides, the valence changes of the A-site Cu and the B-site Fe in the compound were realized by the temperature-induced charge transfer. As a result, a very rare Cu^{3+} state was stabilized at the square-coordinated A sites in the ground state [16, 17]. A similar charge transfer was also found in the isostructural $BiCu_3Fe_4O_{12}$ but at a higher transition temperature [18]. This paper reviews the newly discovered intermetallic charge transfer phenomenon found in A-site-ordered double perovskites.

2. Experimental

Polycrystalline samples of $LaCu_3Fe_4O_{12}$ and $BiCu_3Fe_4O_{12}$ were prepared by solid-state reaction under high pressure (needed to stabilize the special ordered structure). La_2O_3/Bi_2O_3, CuO and Fe_2O_3 were finely mixed at a mole ratio of 1 : 6 : 4 with an appropriate amount of the oxidizing agent $KClO_4$, and then held at 1300–1400 K for 1 h under 10 GPa in a cubic-anvil-type high-pressure apparatus. Using a dilute acid solution to wash away the residual KCl and unreacted starting materials yielded almost single-phase samples.

Phase identification and structure analysis were carried out by x-ray and neutron diffraction. High-resolution synchrotron x-ray diffraction (SXRD) was performed at BL02B2 in SPring-8 with powder samples that were put into glass capillary tubes and rotated during the measurements. A large Debye–Scherrer camera with an imaging plate detector was used, and the 2θ angle range from 1° to 75° was measured with 0.01° resolution. The wavelength used for the measurements on $LaCu_3Fe_4O_{12}$ was 0.77747 Å, and the diffraction data for this compound were collected at 100, 300 and 450 K. The wavelength used for the measurements on $BiCu_3Fe_4O_{12}$ was 0.77785 Å, and the data for this material were collected at 300, 350, 375, 400, 420, 440, 460 and 480 K. Conventional XRD was also performed using a Rigaku x-ray diffractometer with Cu-Kα radiation at temperatures from 173 to 523 K. Neutron powder

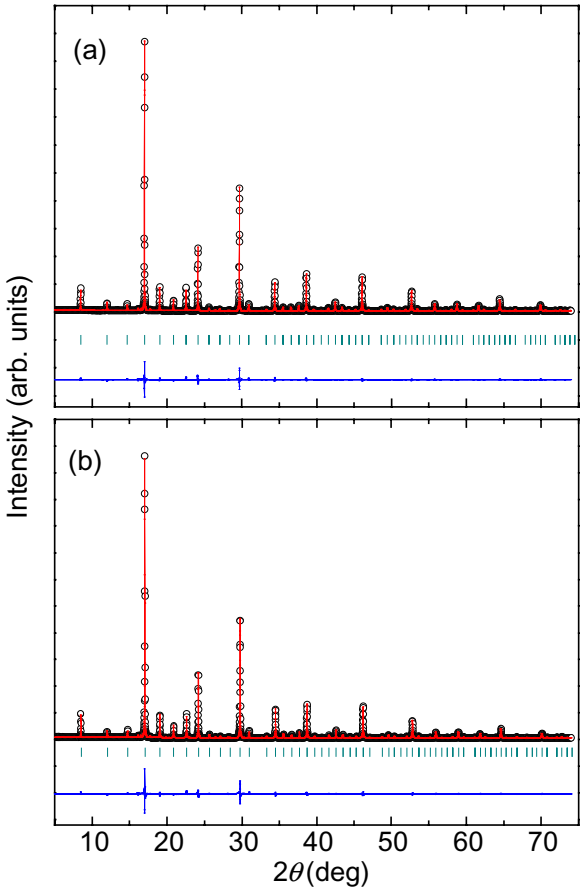

Figure 2. SXRD patterns and the Rietveld refinement profiles of $LaCu_3Fe_4O_{12}$ at (a) 300 K and (b) 450 K. The observed (circles), calculated (red line) and difference (blue line) patterns are shown. The ticks show the positions of the Bragg reflections.

diffraction (NPD) was carried out at the beamline Super-D2B in Institut Laue-Langevin with powder samples in a vanadium can of 5 mm diameter. The 2θ angle range from 5° to 155° was measured using a wavelength of 1.594 Å, and diffraction data were collected at 50, 125, 200, 300, 325, 350, 375, 400 and 425 K. GSAS software was used to refine both the crystal and the magnetic structural parameters [19].

The oxygen content was estimated from the change in the sample weight during the decomposition of the compound. Thermogravimetry (TG) and differential thermal analysis (DTA) measurements from room temperature (RT) to 1200 K were made, at a heating rate of 10 K min^{-1} and in an ambient atmosphere, using a Rigaku TG-DTA 8120 system.

The Fe oxidation states were studied by ^{57}Fe Mössbauer spectroscopy in transmission geometry with a ^{57}Co/Rh γ-ray source in combination with a constant-acceleration spectrometer. The source velocity was calibrated by pure α-Fe. The obtained spectra were fitted by using a least-square method with Lorentzian functions.

Magnetic susceptibility (χ) and magnetization were measured using a Quantum Design superconducting quantum interference device magnetometer in the zero-field cooling mode, and a conventional method was used to measure the electrical resistance.

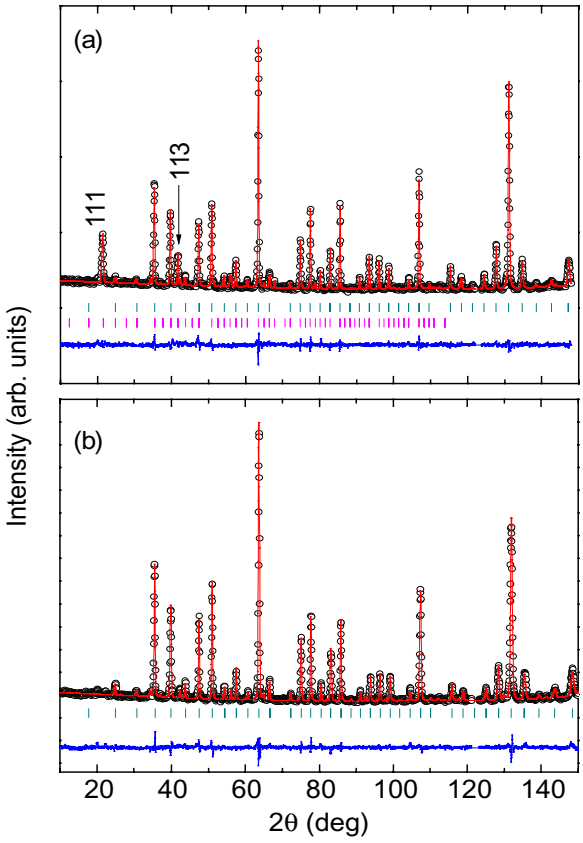

Figure 3. NPD patterns and the Rietveld refinement profiles of $LaCu_3Fe_4O_{12}$ at (a) 300 K and (b) 425 K. The observed (circles), calculated (red line) and difference (blue line) patterns are shown. The green ticks show the positions of the Bragg reflections, and the pink ticks in (a) show the positions of the magnetic reflections from the G-type antiferromagnetic ordering of the B-site spins.

3. Results and discussion

3.1. Crystal structure of $LaCu_3Fe_4O_{12}$ at 300 K

The SXRD and NPD patterns of $LaCu_3Fe_4O_{12}$ at 300 K (figures 2(a) and 3(a), respectively) can be well fitted based on an A-site-ordered double perovskite structure model with a cubic *Im*-3 space group. The NPD data include a magnetic contribution that we discuss in section 3.3. In the structure, A′-site La and A-site Cu are 1 : 3 ordered at special sites 2*a* (0, 0, 0) and 6*b* (0, 0.5, 0.5), respectively. B-site Fe occupies special site 8*c* (0.25, 0.25, 0.25) and O occupies site 24*g* (*x*, *y*, 0). No anomalies in occupation factors at any of the sites were observed in the refinements, suggesting the stoichiometric composition of the material. No oxygen deficiency was observed, even in the refinement with NPD data, which are highly sensitive to oxygen.

The oxygen stoichiometry was further confirmed by the TG measurement results shown in figure 4. The sample decomposed at ≈820 K, losing 3.25% of its mass. The residual products were $LaFeO_3$, $CuFe_2O_4$ and CuO, so the decomposition reaction was $LaCu_3Fe_4O_{12} \rightarrow LaFeO_3 + 3/2CuFe_2O_4 + 3/2CuO + 3/4O_2$. The observed 3.25% weight loss agrees well with the change expected from this reaction (3.22%). All the results obtained in the structure analysis

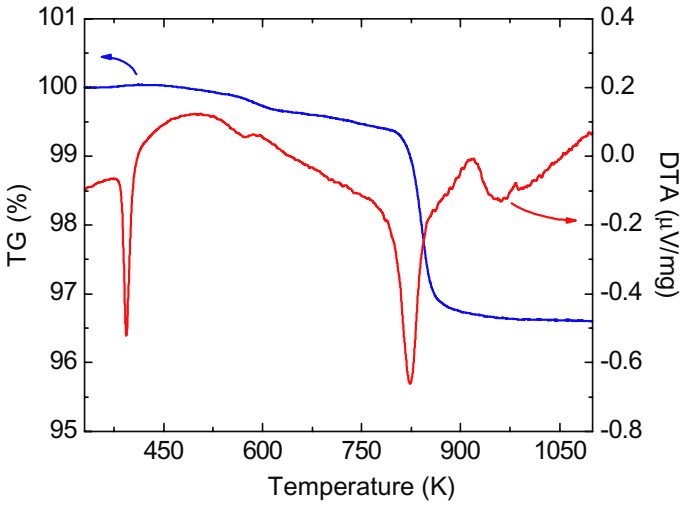

Figure 4. Thermogravimetry and differential thermal analysis of $LaCu_3Fe_4O_{12}$.

Table 1. $LaCu_3Fe_4O_{12}$ and $BiCu_3Fe_4O_{12}$ crystal structure parameters determined by Rietveld refinements of SXRD and NPD data. Numbers in parentheses are standard deviations of the last signigicant digit.

$LaCu_3Fe_4O_{12}$ $BiCu_3Fe_4O_{12}$	SXRD	SXRD	NPD	NPD	SXRD
T (K)	300	450	300	425	300
Space group	*Im*-3	*Im*-3	*Im*-3	*Im*-3	*Im*-3
Z	2	2	2	2	2
a (Å)	7.432 83(4)	7.414 20(6)	7.435 1(1)	7.414 0(1)	7.433 22(8)
V (Å^3)	410.641(7)	407.561(9)	411.02(2)	407.53(2)	410.71(1)
O_x	0.311 1(3)	0.307 0(4)	0.311 0(2)	0.306 3(2)	0.318 7(8)
O_y	0.171 1(4)	0.176 4(4)	0.169 0(3)	0.174 1(3)	0.174 2(5)
U_{iso}(La/Bi) (100 × Å^2)	0.26(2)	0.42(2)	0.5(1)	0.1(1)	3.73(5)
U_{iso}(Cu) (100 × Å^2)	1.09(2)	1.48(3)	1.19(6)	1.64(6)	1.09(5)
U_{iso}(Fe) (100 × Å^2)	0.14(2)	0.22(2)	0.79(3)	0.91(3)	0.09(4)
U_{iso}(O) (100 × Å^2)	0.36(7)	0.67(8)	0.80 (3)	1.13(3)	1.0 (1)
Cu–O (Å) (×4)	1.895(2)	1.939(3)	1.885(2)	1.931(2)	1.869(4)
(×4)	2.819(3)	2.794(4)	2.834(2)	2.811(3)	2.796(4)
(×4)	3.364(6)	3.307(7)	3.377(2)	3.316(6)	3.379(5)
Fe–O (Å) (×6)	2.000 7(9)	1.978(1)	2.005 9(7)	1.981 4(6)	2.008(1)
Fe–O–Fe (deg)	136.5(1)	139.2(2)	135.8(1)	138.6(1)	135.5(2)
R_{wp} (%)	6.70	7.71	5.09	5.12	4.63
R_p (%)	4.70	5.42	4.31	4.12	3.28

and the TG measurement indicate that the compound we made was an A-site-ordered double perovskite with the chemical composition $LaCu_3Fe_4O_{12}$.

The structure parameters and selected bond distances and angles obtained in the final refinements are listed in table 1. The results obtained from SXRD and NPD data are essentially the same. Fe at the B site is coordinated by six oxygen atoms about 2.00 Å away. Bond valence

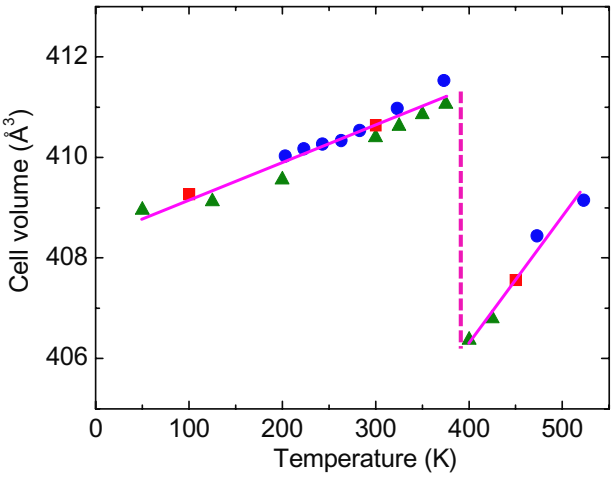

Figure 5. Temperature dependence of the unit cell volume of $LaCu_3Fe_4O_{12}$. The data were obtained from conventional XRD (●), SXRD (■) and NPD (▲).

sums (BVS) [20][3], which empirically give an ionic state of the cation from the bond distances to the coordinated anions, give 3.05 (SXRD) and 3.01 (NPD) for Fe, indicating an Fe^{3+} ionic state in the octahedron. Four short Cu–O bonds in the originally 12-fold-coordinated site make the AO_4 unit. The BVS for the A-site Cu are 2.90 (SXRD) and 2.95 (NPD). The results strongly suggest that an unusual Cu^{3+} with square planar coordination is stabilized in the A-site-ordered structure and that at 300 K the charge combination is $LaCu_3^{3+}Fe_4^{3+}O_{12}$.

3.2. Isostructural phase transition

When the sample was heated, DTA showed a sharp endothermic peak at 393 K, whereas TG showed no change (figure 4). Here we define this temperature as a critical phase transition temperature (T_c) in $LaCu_3Fe_4O_{12}$.

Figures 2(b) and 3(b), respectively, show high-temperature SXRD (450 K) and NPD (425 K) patterns of $LaCu_3Fe_4O_{12}$. Note that the crystal symmetry of the phase above T_c is the same as that of the phase below T_c, suggesting that the phase transition is an isostructural one. The structural parameters obtained in the refinements are also listed in table 1. Above T_c the Cu–O distance in the A-site square unit was significantly greater than it was below T_c, whereas the Fe–O distance in the BO_6 octahedron was considerably less than it was below T_c. As a result, the BVS values for the A-site Cu decreased to 2.06 (SXRD) and 2.08 (NPD), while those for the B-site Fe increased to 3.44 (SXRD) and 3.41 (NPD). The results indicate that the Cu valence is 2+, a typical value for the square planar coordination, and that the Fe valence is unusually high. Since the TG measurement showed no apparent weight loss at temperatures up to 500 K (figure 4), it is reasonable to conclude that the oxygen content of the material was stoichiometric at temperatures between 425 and 450 K. A simple ionic valence calculation indicates that the high-temperature charge combination is $LaCu_3^{2+}Fe_4^{3.75+}O_{12}$, which is the same as that of other A-site-ordered double perovskites, like $LaCu_3^{2+}Mn_4^{3.75+}O_{12}$ [7] and $BiCu_3^{2+}Mn_4^{3.75+}O_{12}$ [8].

[3] The BVS values (V_i) for Cu, Fe and Bi ions were calculated using the formula $V_i = \sum_j S_{ij}$ and $S_{ij} = \exp[(r_0 - r_{ij})/0.37)]$. The following r_0 values were used: 1.739 and 1.649, respectively, for Cu^{3+} and Cu^{2+} with 12 coordinated oxygen atoms; 1.751 and 1.772, respectively, for Fe^{3+} and $Fe^{3.75+}$ with 6 coordinated oxygen atoms.

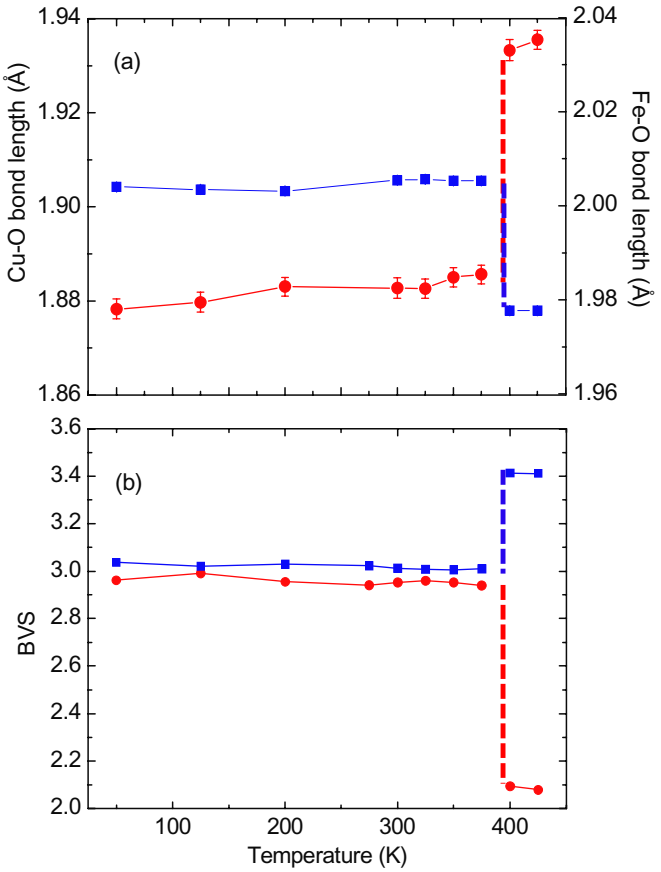

Figure 6. Temperature dependence of (a) Cu–O (●) and Fe–O (■) bond lengths and (b) calculated BVS values for Cu (●) and Fe (■) ions in $LaCu_3Fe_4O_{12}$.

The temperature dependence of the unit cell volume (a^3) of $LaCu_3Fe_4O_{12}$ (figure 5) shows a sharp change at the transition temperature, indicating that the transition is a first-order one. The normal volume expansion with increasing temperature was interrupted by a 1.2% volume contraction at the phase transition temperature. This unusual volume contraction was mainly due to the significant reduction in the length of the Fe–O bond (figure 6(a)). The length of the Cu–O bond increased correspondingly because oxygen atoms are bonded to both Cu in the square units and Fe in the octahedral units, but this bond does not make the structural framework.

The above structural change suggests that the charge combination changes from $LaCu_3^{3+}Fe_4^{3+}O_{12}$ below T_c to $LaCu_3^{2+}Fe_4^{3.75+}O_{12}$ above T_c. This is clear from the change in the BVS values for Cu and Fe (figure 6(b)). The simultaneous valence variations of Cu and Fe imply a temperature-induced intermetallic charge transfer between the A-site Cu and the B-site Fe: $3Cu^{3+} + 3e^- \rightarrow 3Cu^{2+}$ and $4Fe^{3+} - 3e^- \rightarrow 4Fe^{3.75+}$. At T_c, electrons released from the B-site Fe^{3+} ions move to the A-site Cu^{3+} ions, reducing Cu^{3+} to Cu^{2+}.

3.3. Antiferromagnetism-to-paramagnetism transition

The ionic state changes caused by the intermetallic charge transfer change the magnetic states of the ions. Mössbauer spectroscopy provides useful information on the valence state and spin state of Fe ions, and figure 7 shows the Mössbauer spectra (MS) of $LaCu_3Fe_4O_{12}$ at 4.2, 298

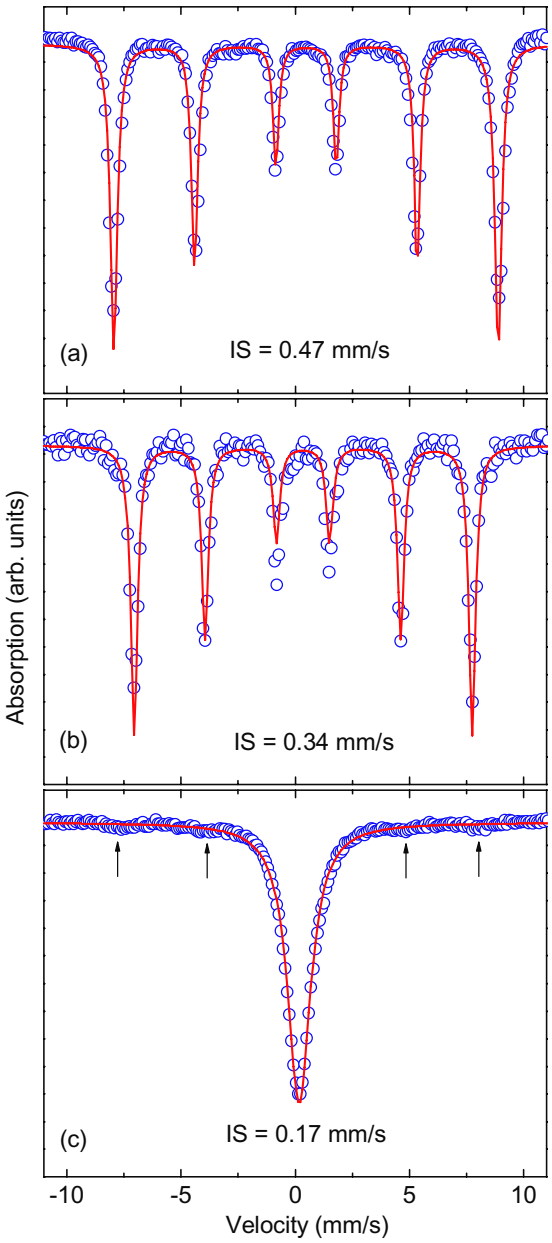

Figure 7. MS of $LaCu_3Fe_4O_{12}$ at (a) 4.2 K, (b) 298 K and (c) 423 K. Arrows in (c) show spectral features due to a small amount of α-Fe_2O_3 impurity.

and 423 K. The MS at 4.2 and 298 K are quite similar and show a single magnetic sextuplet component at each temperature. The isomer shift (IS) values at 4.2 and 298 K were, respectively, 0.47 and 0.34 mm/s, which are typical values for Fe^{3+} with a high-spin configuration [21, 22], further confirming the charge formula of $LaCu_3^{3+}Fe_4^{3+}O_{12}$ below the transition temperature. The observed magnetic sextuplet indicates that the Fe spins below T_c were magnetically ordered and that there was no other magnetic transition than that at T_c.

The NPD pattern of $LaCu_3Fe_4O_{12}$ at 300 K (figure 3(a)) included magnetic reflections in addition to the nuclear peaks, so we can determine the magnetic structure. As clearly seen in the 111 and 113 Bragg reflections, strong magnetic contributions were observed. The refinement

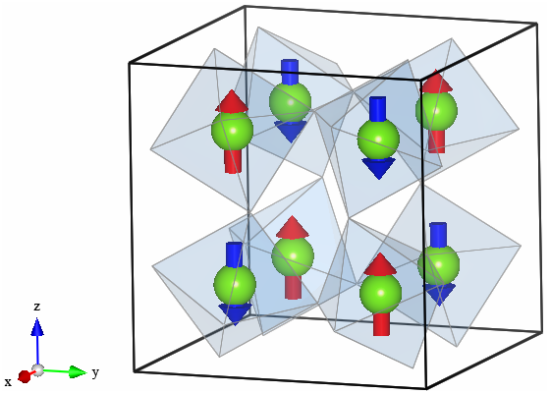

Figure 8. The G-type antiferromagnetic structure of B-site Fe^{3+} spins in $LaCu_3Fe_4O_{12}$. Only the magnetic ordered Fe^{3+} ions are shown. The spins are drawn along the [001] direction because the exact orientation of the magnetic moments cannot be determined by NPD.

revealed a magnetic superstructure with a (1/2 1/2 1/2) propagation vector of the cubic cell, which gave a G-type antiferromagnetic ordered structure. Thus, each Fe^{3+} spin aligns antiparallel to the six nearest neighbors, as shown in figure 8. No magnetic contribution from the square-planar-coordinated 6*c* site was found. Because the square-planar-coordinated Cu gives rise to a considerable energy splitting between $d_{x^2-y^2}$ and $d_{3z^2-r^2}$ orbitals, the 3d electrons in Cu^{3+} ($3d^8$) ions fully occupy the d_{xz}, d_{yz}, d_{xy} and $d_{3z^2-r^2}$ orbitals, making the $d_{x^2-y^2}$ orbital empty with an $S = 0$ spin state. The refined magnetic moment of the B-site Fe at 50 K was 4.03(2) μ_B, which was reduced from the ideal value of 5 μ_B for high-spin Fe^{3+} ($S = 5/2$), probably by a covalency effect. The antiferromagnetic ordering thus originates from Fe–O–Fe superexchange interactions. Linear behaviors in the field dependence of magnetization below T_c (inset of figure 9(a)) were also consistent with an antiferromagnetic ordered state of the spins. The result also agrees with a recent density functional analysis, which gives the G-type antiferromagnetic spin ordering in the ground state [23].

When increasing the temperature, the compound changed from an antiferromagnet to a paramagnet at T_c. The MS at 423 K (figure 7(c)) consisted of a paramagnetic singlet with an IS of 0.17 mm s^{-1}, which is an intermediate value between ≈0.07 mm s^{-1} for an Fe^{4+} state and ≈0.35 mm s^{-1} for an Fe^{3+} state [24, 25]. The absence of a magnetic contribution was confirmed in the NPD pattern obtained at 425 K. The temperature dependence of the magnetic susceptibility, hyperfine field (HF) in MS and spin moment of Fe^{3+} obtained from the NPD data is plotted in figure 9. The anomaly in χ–T at T_c corresponds to an antiferromagnetism-to-paramagnetism transition, and the small increase in χ at low temperature is probably due to the small amount of indiscernible paramagnetic impurities. The HF in MS decreased gradually with increasing temperature and, at T_c, fell to zero. The obtained magnetic moment of Fe from NPD refinement, 4.03(2) μ_B at 50 K, similarly decreased gradually to 3.28(3) μ_B at 375 K and then fell to zero when the intermetallic charge transfer transition occurred. The magnetic transition at T_c was of first order and was not a normal thermal evolution of the magnetic moment. The spin fluctuations do not result from valence fluctuations as the charge transfer transition is approached, but instead they reflect the intrinsic strength of the magnetic interaction between the Fe spins that would determine the antiferromagnetic Néel temperature if the intermetallic charge

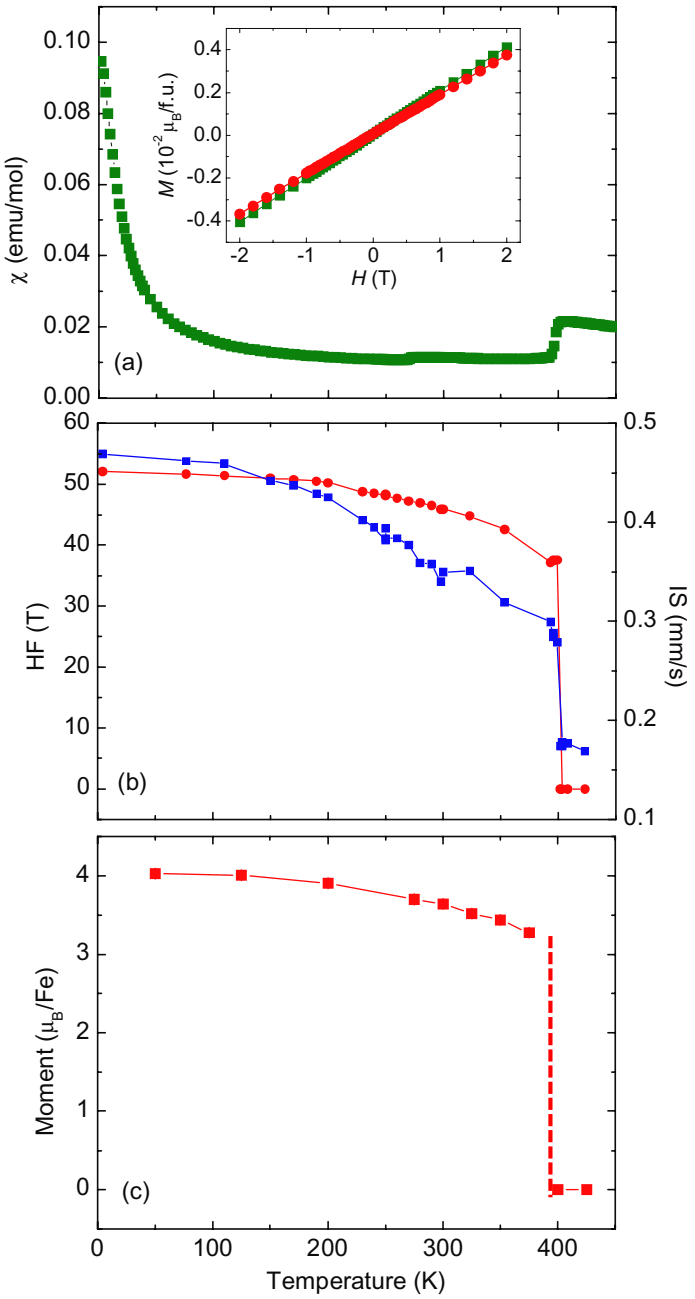

Figure 9. Temperature dependence of (a) magnetic susceptibility χ measured at an applied field of 0.1 T, (b) hyperfine field HF (●) and isomer shift IS (■) and (c) magnetic moment of Fe obtained from NPD analysis of $LaCu_3Fe_4O_{12}$. The inset in (a) shows the linear magnetization behavior at 300 K (●) and 200 K (■).

transfer did not occur. Fitting an $S = 5/2$ Brillouin function to the moments obtained from NPD data yielded a projected Néel temperature of $\approx$600 K. These results demonstrate that energy scales of the spin and charge transfer degrees of freedom in $LaCu_3Fe_4O_{12}$ are significantly different and that the intrinsic magnetic superexchange interaction of Fe^{3+} spins is much larger

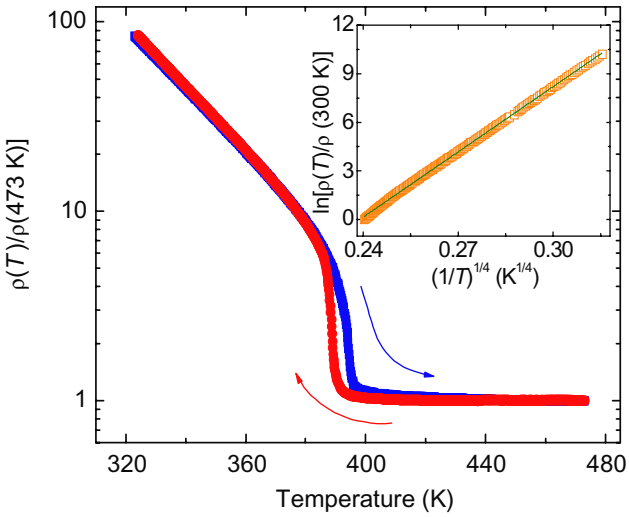

Figure 10. Temperature dependence of normalized resistivity of $LaCu_3Fe_4O_{12}$. The inset shows the result obtained by fitting data in the temperature range between 100 and 300 K to a 3D VRH model.

than the apparent magnitude of $\approx k_B T_c$, even though the intermetallic charge transfer drives the actual antiferromagnetism-to-paramagnetism transition at 393 K.

3.4. Insulator-to-metal transition

In accordance with the cation valence changes due to the intermetallic charge transfer, the electronic properties of the compound also changed. In the A-site-ordered double perovskites, the AO_4 units are spatially isolated from each other, and the electrical properties are thus determined mainly by the corner-sharing BO_6 octahedral network. As shown in figure 10, the low-temperature phase with Fe^{3+} showed insulating behavior. The temperature dependence of resistance between 100 and 300 K can be fitted using a Mott 3D variable-range hopping (VRH) model: $R(T) = R_0 \exp(T_0/T)^{1/4}$ (inset of figure 10). An insulator-to-metal transition occurred at T_c, and the observed thermal hysteresis in resistance is in agreement with the first-order nature of the intermetallic charge transfer transition. Above T_c the mixed valence state of the B-site $Fe^{3.75+}$ made the compound metallic.

The insulator-to-metal transition in $LaCu_3Fe_4O_{12}$ is different from those observed in TM oxides with a simple perovskite structure. Chemical doping by substitution is a conventional way of modulating the carrier concentration and/or the width of bands of TM ions, which often gives rise to an insulator-to-metal transition [26]. In the present A-site-ordered double perovskite $LaCu_3Fe_4O_{12}$, in contrast, the insulator-to-metal transition is a result of the intermetallic charge transfer between the A-site Cu and B-site Fe changing the electronic states of these two cations simultaneously. This change in electronic structure can be regarded as an 'internal doping' between Cu and Fe without involving any external doping elements.

3.5. Intermetallic charge transfer in $BiCu_3Fe_4O_{12}$

$BiCu_3Fe_4O_{12}$ also crystallized with the A-site-ordered perovskite structure. The structural parameters of $BiCu_3Fe_4O_{12}$ that were refined from SXRD data taken at 300 K are listed in

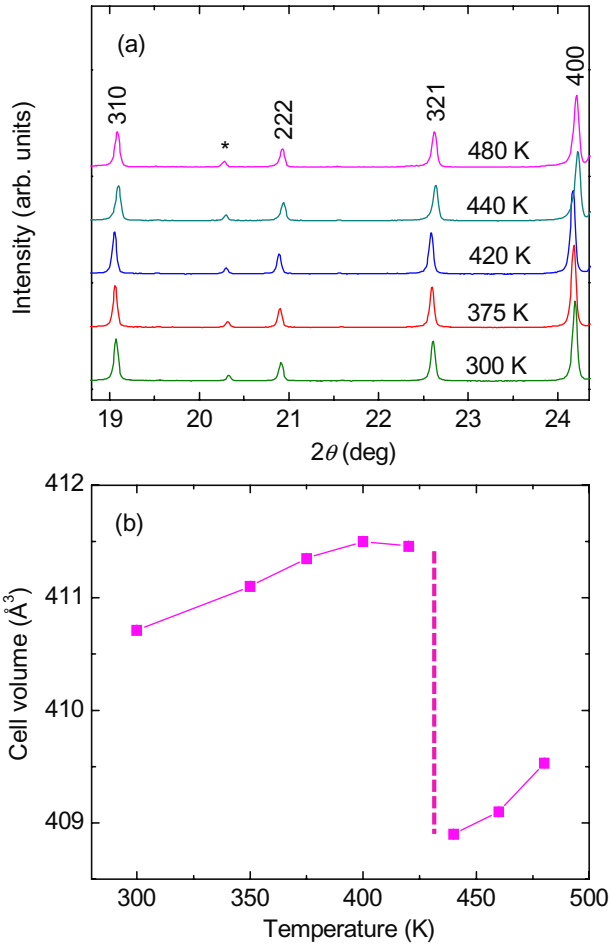

Figure 11. Changes in (a) SXRD patterns and (b) unit cell volume of $BiCu_3Fe_4O_{12}$. In (a) the peak marked with an asterisk is due to an α-Fe_2O_3 impurity.

table 1. Bi^{3+} and La^{3+} have the same formal ionic charges and similar ionic radii [27], but Bi^{3+} has a lone pair of $6s^2$ electrons that often causes crystal structure distortion due to a stereochemical effect. The present A-site-ordered perovskite $BiCu_3Fe_4O_{12}$, however, showed a cubic symmetry and thus Bi^{3+} did not manifest a lone pair effect.

One sees in figure 11 that $BiCu_3Fe_4O_{12}$, like $LaCu_3Fe_4O_{12}$, showed an isostructural phase transition associated with a volume contraction. The contraction was smaller (about 0.6%), however, and occurred at a higher temperature (between 420 and 440 K). The lengths of the Cu–O bonds in the square-planar-coordinated CuO_4 unit and the Fe–O bonds in the FeO_6 octahedron changed significantly at the transition temperature (figure 12(a)). The valence states of Cu and Fe calculated from BVS changed correspondingly (figure 12(b)), indicating that an intermetallic charge transfer occurred and that the compound changed from $BiCu_3^{3+}Fe_4^{3+}O_{12}$ below T_c to $BiCu_3^{2+}Fe_4^{3.75+}O_{12}$ above T_c. The temperature dependences of magnetic susceptibility and normalized resistivity (figure 13) show that the intermetallic charge transfer transition also causes antiferromagnetism-to-paramagnetism and insulator (semiconductor)-to-metal transitions.

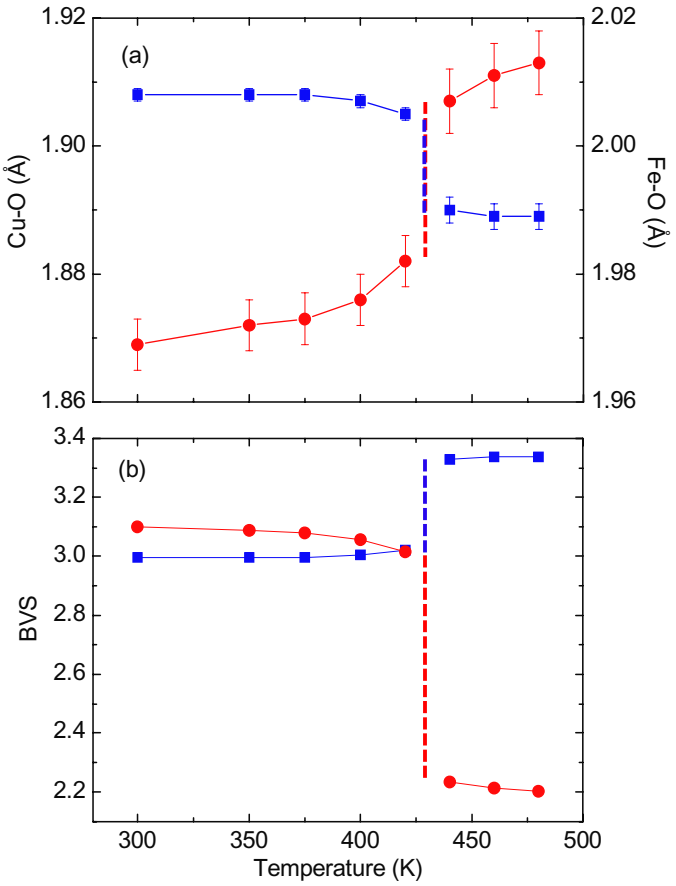

Figure 12. Temperature dependence of (a) Cu–O (●) and Fe–O (■) bond lengths and (b) BVS for Cu (●) and Fe (■) ions in $BiCu_3Fe_4O_{12}$.

The transition temperature obtained from the temperature derivative of the susceptibility was 428 K, which was higher than that of $LaCu_3Fe_4O_{12}$. This implies that the Cu^{3+} state in the square planar coordination at the A sites is more stable in $BiCu_3Fe_4O_{12}$ than in $LaCu_3Fe_4O_{12}$. Because 6s and 6p orbitals in Bi often hybridize with 2p orbitals in O in oxides, the stabilization of Cu^{3+} may be mediated through the orbital hybridization in Bi–O–Cu bonds. Although the Bi cations at the A sites do not take part in the charge transfer, they play a role in stabilizing the square-planar-coordinated Cu^{3+} and thereby increase the intermetallic charge transfer transition temperature.

3.6. Charge transfer and charge disproportionation

Ca^{2+} substitution at the A′ sites produced another A-site-ordered double perovskite, $CaCu_3Fe_4O_{12}$, but this compound showed a completely different transition: charge disproportionation [28]. When this compound is cooled, at 210 K the unusually high valence state of the Fe^{4+} ions at the B sites is resolved by a charge disproportionation from Fe^{4+} to Fe^{3+} and Fe^{5+} in a phase transition from $CaCu_3Fe_4^{4+}O_{12}$ to $CaCu_3(Fe_2^{3+}Fe_2^{5+})O_{12}$. This charge disproportionation is similar to that seen in the distorted orthorhombic perovskite $CaFeO_3$ [25]. In the present $(La/Bi)Cu_3Fe_4O_{12}$, on the other hand, the instability of the unusually high valence

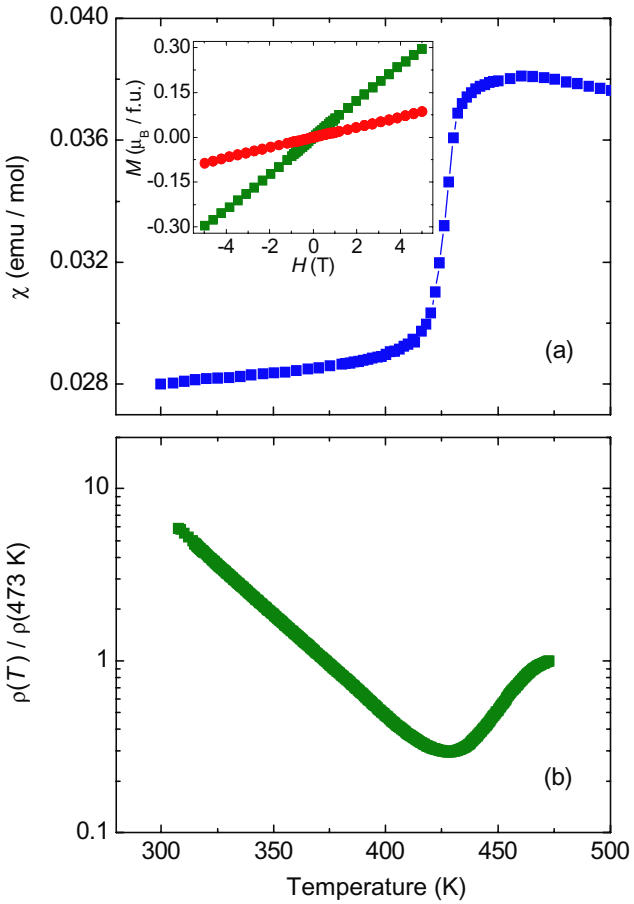

Figure 13. Temperature dependence of (a) magnetic susceptibility χ measured at an applied field of 0.1 T and (b) normalized resistance of $BiCu_3Fe_4O_{12}$. The inset in (a) shows the linear magnetization behavior at 5 K (●) and 300 K (■).

$Fe^{3.75+}$ ions at high temperature was resolved by the charge transfer between the A-site Cu and the B-site Fe. Note that $CaCu_3Fe_4O_{12}$ and $(La/Bi)Cu_3Fe_4O_{12}$ differ at only one-fourth of the A sites in simple ABO_3 perovskite compositions.

The unusually high valence states of TM ions like Fe^{4+} and Cu^{3+} in oxides have very low-lying 3d levels and thus make covalent electronic states with ligand holes L [29]. The charge disproportionation in $CaCu_3Fe_4O_{12}$ ($2Fe^{4+} \rightarrow Fe^{3+} + Fe^{5+}$) is thus expressed as ($2d^5L \rightarrow d^5 + d^5L^2$), and the disproportionation at 210 K is thought to be due to the redistribution of the ligand holes in the Fe–O bonds. This redistribution makes the Fe–O bonds alternately shorter and longer, producing the 1 : 1 rock-salt-type ordering with *Pn*-3 symmetry, which appears to be a reasonable way to minimize the lattice energy. In $(La/Bi)Cu_3Fe_4O_{12}$ with the fractional 3.75+ state of Fe, on the other hand, charge disproportionation ($8Fe^{3.75+} \rightarrow 5Fe^{3+} + 3Fe^{5+}$) may be possible but the large lattice energy makes it hard to form a simple ordered redistribution of the ligand holes. Instead, the intermetallic charge transfer between the A-site Cu ions and the B-site Fe ions ($3Cu^{2+} + 4Fe^{3.75+} \rightarrow 3Cu^{3+} + 4Fe^{3+}$) is mediated by the redistribution of the ligand holes from the Fe–O bonds to the Cu–O bonds ($3d^9 + 4d^5L^{0.75} \rightarrow 3d^9L + 4d^5$) while keeping the cubic *Im*-3 symmetry. The redistribution of the ligand holes from the Fe–O bonds to the Cu–O bonds does not need much energy because all the oxygen atoms in the A-site-ordered

double perovskite structure are shared by the FeO_6 octahedra and the CuO_4 square-planar units. Thus, the intermetallic charge transfer energy overcomes the charge disproportionation energy in (La/Bi)$Cu_3Fe_4O_{12}$ and the unusually high valence state of $Fe^{3.75+}$ is resolved by the intermetallic charge transfer at a low temperature [30].

4. Summary

A temperature-induced Cu–Fe intermetallic charge transfer phenomenon found in A-site-ordered double perovskites $RCu_3Fe_4O_{12}$ (R = La, Bi) was reviewed. The materials were prepared under high-pressure and high-temperature conditions. In the ground state a very rare Cu^{3+} state was stabilized at the square-planar-coordinated A sites and the charge combination was $RCu_3^{3+}Fe_4^{3+}O_{12}$. With increasing temperature, intermetallic charge transfer between the A-site Cu and the B-site Fe took place at 393 K for $LaCu_3Fe_4O_{12}$ and 428 K for $BiCu_3Fe_4O_{12}$, changing the charge combination to $RCu_3^{2+}Fe_4^{3.75+}O_{12}$. The energy levels of the unusually high Cu^{3+} and $Fe^{3.75+}$ states were comparable so that changing the temperature triggered the intermetallic charge transfer. This charge transfer resulted in a first-order isostructural phase transition accompanied by a large contraction of unit cell volume and by antiferromagnetism-to-paramagnetism and insulator-to-metal transitions. Substitution of Bi for La stabilized the Cu^{3+} state at the square-planar-coordinated A sites and raised the intermetallic charge transfer transition temperature.

Acknowledgments

We thank W T Chen, T Saito, M Azuma, N Hayashi and J P Attfield for their help with the experiments and for fruitful discussions. This work was partly supported by the Global COE Program (no. B09), Grants-in-Aid for Scientific Research (nos 19GS0207, 18350097 and 17105002) and a grant for the Joint Project of Chemical Synthesis Core Research Institutions from MEXT of Japan. The synchrotron radiation experiments were performed at SPring-8 with the approval of the Japan Synchrotron Radiation Research Institute. The neutron diffraction experiment was done under the Strategic Japanese-UK Cooperative Program by JST/EPSRC.

References

[1] Vasil'ev A N and Volkova O S 2007 *Low Temp. Phys.* **33** 895
[2] Shimakawa Y 2008 *Inorg. Chem.* **47** 8562
[3] Subramanian M A, Li D, Duan N, Reisner B A and Sleight A 2000 *J. Solid State Chem.* **151** 323
[4] Ramirez A P *et al* 2000 *Solid State Commun.* **115** 217
[5] Homes C C, Vogt T, Shapiro S M, Wakimoto S and Ramirez A 2001 *Science* **293** 673
[6] Zeng Z, Greenblatt M, Subramanian M A and Croft M 1999 *Phys. Rev. Lett.* **82** 3164
[7] Alonso J A *et al* 2003 *Appl. Phys. Lett.* **83** 2623
[8] Takata K, Yamada I, Azuma M, Takano M and Shimakawa Y 2007 *Phys. Rev.* B **76** 024429
[9] Shiraki H *et al* 2007 *Phys. Rev.* B **76** 140403
[10] Shimakawa Y, Shiraki H and Saito T 2008 *J. Phys. Soc. Japan* **77** 113702
[11] Prodi A *et al* 2004 *Nat. Mater.* **3** 48
[12] Tohyama T *et al* 2010 *Inorg. Chem.* **49** 2492
[13] Imamura N, Karppinen M, Motohashi T, Fu D, Itoh M and Yamauchi H 2008 *J. Am. Chem. Soc.* **130** 14948

[14] Mezzadri F *et al* 2009 *Phys. Rev.* B **79** 100106
[15] Long Y W, Saito T, Mizumaki M, Agui A and Shimakawa Y 2009 *J. Am. Chem. Soc.* **131** 16244
[16] Long Y W, Hayashi N, Saito T, Azuma M, Muranaka S and Shimakawa Y 2009 *Nature* **458** 60
[17] Chen W T *et al J. Mater. Chem.* DOI:10.1039/C0JM00767F
[18] Long Y W, Saito T, Tohyama T, Oka K, Azuma M and Shimakawa Y 2009 *Inorg. Chem.* **48** 8489
[19] Larson A C and von Dreele R B 1994 General Structure Analysis System (GSAS) *Report No.* LAUR 86-748 (Los Alamos National Laboratory)
[20] Brown I D and Altermatt D 1985 *Acta Crystallogr.* B **41** 244
[21] Li X *et al* 1991 *Hyperfine Interact.* **69** 851
[22] Blaauw C and Van der Woude F 1973 *J. Phys. C: Solid State Phys.* **6** 1422
[23] Lee C, Kan E and Whangbo M-H 2009 arXiv:0904.4809v1
[24] Kawasaki S, Takano M and Takeda Y 1996 *J. Solid State Chem.* **121** 174
[25] Takano M *et al* 1977 *Mater. Res. Bull.* **12** 923
[26] Imada M, Fujimori A and Tokura Y 1998 *Rev. Mod. Phys.* **70** 1039
[27] Shannon R D 1976 *Acta Crystallogr.* A **32** 751
[28] Yamada I *et al* 2008 *Angew. Chem. Int. Ed. Engl.* **47** 7032
[29] Bocquet A E *et al* 1992 *Phys. Rev.* B **45** 1561
[30] Shimakawa Y and Takano M 2009 *Z. Anorg. Allg. Chem.* **635** 1882